Analytical inverse solution for coupled thermoelastic problem for the evaluation of contact stress during steel strip rolling

Daniel Weisz-Patrault, Alain Ehrlacher, Nicolas Legrand

Analytical inverse solution for coupled thermoelastic problem for the evaluation of contact stress during steel strip rolling

Daniel Weisz-Patrault[a], Alain Ehrlacher[a], Nicolas Legrand[b]

[a]*Ecole Ponts ParisTech, UR Navier, 6 & 8 Ave Blaise Pascal, 77455 Marne La Vallee, France*
[b]*ArcelorMittal Global Research & Development, Maizière Process Voie Romaine, BP 30320 F-57283 Maizières-lès-Metz Cedex*

Abstract

Knowledge of the contact stress between roll and strip is a critical factor in modern, high-speed rolling mills. Previously two inverse analytical methods have been developed to determine the elastic contact stress on the one hand and the heat flux or the temperature in the whole roll (and especially at the surface) on the other hand, by measuring the stress tensor inside the roll body with fibre optics and by measuring the temperature with a thermocouple fully embedded at only one point inside the roll. However measurements done by fibre optics take into account the elastic stress and the thermal stress. However the contact stress was determined under isothermal assumption, which is strongly incorrect for hot rolling conditions. In this paper, the coupled thermoelastic problem is solved analytically using the theorem of superposition and the expression of the temperature field exhibited previously. A significant improvement of the accuracy of the inverse method for reconstructing the contact stress is observed by taking into account thermal stress. Hot rolling simulation is given to demonstrate this result. The computation time is studied to rapidly optimise the industrial parameters during the rolling process, and considering that both inverse methods have been run, the computation of thermal stress does not cost significant additional CPU times.

Keywords:
Steel rolling, Thermoelastic, Friction sensor, Computation time, Inverse analysis, Temperature sensor

Table 1: Nomenclature

Roll	
R_d	Radius of the roll
R_c	Radius of temperature measurements (thermocouple)
R_b	Radius of stress measurements (fibre optics)
r	Radial position of Eulerian point
θ	Angular position of Eulerian point
t	Time
T_a	Initial temperature of the roll
$\boldsymbol{e_r}$	Radial direction
$\boldsymbol{e_\theta}$	Circumferential direction
ω	Rotation speed
D	Thermal diffusivity of the roll
α	Thermal dilatation of the roll
α_F	Thermal dilatation of the fibre optics
λ, μ	Lamé's coefficients of the roll
Solution in the roll	
T	Eulerian temperature
T_n	nth coefficient involved in the expansion of T (complex)
γ_n	nth coefficient involved in the expansion of T (real)
$\boldsymbol{u}$	Displacement field
u_r	Radial displacement

u_θ	Circumferential displacement
σ	Stress of the global problem
σ^r	Reconstructed stress (global problem)
σ^a	Applied stress (global problem)
σ^A	Stress of the auxiliary problem A
σ^B	Stress of the auxiliary problem B
σ^C	Stress of the auxiliary problem C
σ^{th}	Thermal stress ($\sigma^{th} = \sigma^A + \sigma^B$)
$\boldsymbol{T}^A$	Tensile vector of the auxiliary problem A
$\boldsymbol{T}^B$	Tensile vector of the auxiliary problem B
$\boldsymbol{T}^C$	Tensile vector of the global problem and problem C
N_1	Order of truncation (integer)
N_2	Order of truncation (integer)
N_θ	Number o points of the reconstruction (integer)
ζ_n	Coefficient (complex)
J_n	nth Bessel function of the first kind
x_n	Successive positive zeros of J_0
$P_n(r)$	Function involved in the expansion of u_r
$p_n(r)$	Function involved in the expansion of u_r
$Q_n(r)$	Function involved in the expansion of u_θ
$q_n(r)$	Function involved in the expansion of u_θ
L_n	Coefficient (complex)
l_n	Coefficient (real)
$\boldsymbol{L}$	Vector of L_n
$\boldsymbol{l}$	Vector of l_n
$l_n(r)$	Coefficient (real)
$S_n(r)$	Function involved in the expansion of σ^A
$s_n(r)$	Function involved in the expansion of σ^A
z	Complex variable $z = r\exp(i\theta)$
$\Phi(z)$	Holomorphic function
$\Psi(z)$	Holomorphic function
$f(z)$	Holomorphic function
$g(z)$	Holomorphic function
ϕ_n	Coefficient of the expansion of $\Phi(z)$
ψ_n	Coefficient of the expansion of $\Psi(z)$
f_n	Coefficient of the expansion of $f(z)$
g_n	Coefficient of the expansion of $g(z)$
$\boldsymbol{\phi}$	Vector of ϕ_n
$\boldsymbol{\psi}$	Vector of ψ_n
$A^{\cdot\cdot}$	Matrices related to σ^A (..=rr, $r\theta$ or $\theta\theta$)
$\boldsymbol{a}^{\cdot\cdot}$	Vectors related to σ^A (..=rr, $r\theta$ or $\theta\theta$)
B_j	Matrices related to σ^B (j=1,2 or 3)
$g_j(r)$	Auxiliary functions (j=1,2,3 or 4)
ϵ	Error estimate
	Strip
T_i	Initial temperature of the strip
F_R	Rolling force
t_i	Initial thickness of the strip
t_f	Final thickness of the strip
R	Reduction ratio of the strip

L_c	Contact length
HTC	Heat Transfer Coefficient in the contact strip/roll
σ_0	Initial yield stress of the strip

1. Introduction

1.1. Objectives of the paper

In steel rolling processes, two rolls are used as tools to reduce the thickness of a workpiece. Modern rolling mills combine higher rolling speeds, larger reductions, harder steel grades and thinner rolled strips. Thus, to ensure better product quality, especially in terms of thickness, flatness and defect-free surface, knowledge of friction and lubrication in the roll gap becomes critical. The contact between the strip and the roll is a location of unknown shear stress and normal pressure and lubrication conditions. Some models that characterise the interface taking into account lubrication have been proposed in recent years by Montmitonnet et al. [1] but still need experimental validation. On the other hand, with industrial rolling process being currently dictated by empiricism, knowledge of the contact stress would be desirable to allow an optimisation of parameters such as speed and lubrication, with a closed-loop control.

In order to estimate the contact stress between the roll and the strip Legrand et al. [2] recently computed an inverse method (with isothermal assumption) developed by Meierhofer and Stelson [3], which interprets stresses measured at two locations inside the roll (at two different radii). Legrand et al. [2] studied the skin thickness where thermal stress is not negligible and attempted to perform the inverse method by measuring the stress tensor deeper than this skin thickness. The inversion failed, and the authors concluded that the inversion was impossible for hot rolling conditions. However, this paper is an attempt to overcome this difficulty. Instead of measuring deeper than the skin thickness to avoid large thermal stress, a thermoelastic problem can be solved to take into account thermal stress and therefore to allow measurements very close from the surface of the roll.

In a previous contribution Weisz-Patrault et al. [4] proposed an improved inverse analytical method which interprets measured stresses (fibre optics fully embedded) to infer the contact stress between the roll and the strip. Measurements are done at only one location inside the roll and the method is demonstrated to be more accurate. The solution is analytical and a very short computation times are obtained (0.07 s for each cycle). To make the reading easier, the basic mathematical principles of the solution are reminded in Section 4. However the problem was assumed to be isothermal. Therefore a corrective solution is needed to take into account the significant thermal stress occurring during hot rolling. It is demonstrated in the paper (Section 9) that it is necessary to take into account this thermal stress, otherwise the error compromises the inverse method.

Weisz-Patrault et al. [5] also proposed an inverse analytical method which interprets measured temperatures (thermocouple fully embedded) to infer heat flux or temperature field in the whole roll (and especially at the surface of the roll without knowing any thermal boundary conditions). The method being analytical very short computation times are also obtained (0.05 s for each cycle) and the basic mathematical principles of the solution are reminded in Section 5.

In this paper, thermal stresses are derived from this temperature field by using analytical developments. Mathematical modeling and analytical solutions are exposed in Sections 6 and 7. Moreover this paper aims at combining both inverse solutions (contact stress and temperature field) in order to obtain the contact stress between the roll and the strip by taking into account large gradients of temperature and therefore large thermal stress.

The Figure 1 presents a schematic view of the measurement system. The thermocouple is located at the radius R_c and the fibre optics at the radius R_b. The rotation of the roll allows measurements on the whole circles.

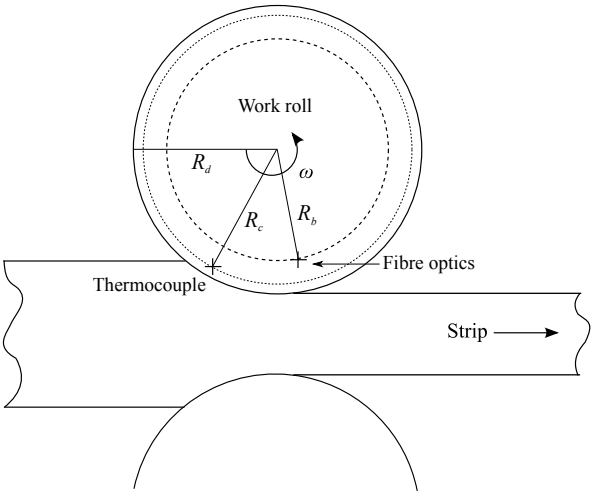

Figure 1: Geometry

1.2. Perspectives

Although the main focus of this paper is the contact stress between the roll and the strip (determined by inverse analysis and corrected with the present thermoelastic problem), the present method can be used for other aims. For hot rolling conditions, knowledge of thermal stress also enables the evaluation of thermal fatigue, which is one of the major factor of wear on rolls. In this way Corral et al. [6] proposed a mixed analytical/numerical model which predicts the life time of the work roll on the base of an analysis of thermal stress. However, the coupling of the radial and tangential displacement is neglected as well as the rotations. The solution proposed by Corral et al. [6] is compared with the solution developed in this paper to show the influence of these simplifications. Li et al. [7] proposed more recently a three-dimensional model by Finite Element Method (FEM) to evaluate the thermal stress of the roll.

1.3. Fibre optics and thermocouple

The fibre optics are glued to the roll body in a thin hole. The thermoelastic stress of the roll body passes through the glue to the fibre optics. The stiffness of the glue implies that a transfer function is necessary to interpret the measurement of the fibre optics. In this paper this transfer function is not studied. Moreover, the variation of temperature of the fibre optics themselves implies an additional measured thermal strain. This additional thermal strain has nothing to do with the additional thermal stress due to the roll body, and should be removed separately. This can be done by considering an axial body (the fibre) loaded by a variation of temperature $\Delta T = T - T_a$. The thermal strain is therefore $\epsilon = \alpha_F \Delta T$, where T is the actual temperature at the position of the fibre, T_a the initial temperature and α_F the thermal dilatation of the fibre. In the following it is assumed that the inputs have been cleaned from this additional thermal strain.

The insertion of the thermocouple in the roll body has been studied experimentally by Weisz-Patrault et al. [8] who focused on the feasibility of inserting a thermocouple in industrial work rolls, technological equipment, wireless acquisition system, quality of measurements and influence of the reduction ratio of the strip. Legrand et al. [9] proposed another experimental study which focuses more especially on the influence of the scale thickness and evaluation of the contact resistance between the strip and the roll.

2. Validation of the method

2.1. Rolling conditions for validation

The validation of the exactness of the analytical solution (which computes thermal stress) on the one hand and the necessity of taking this thermal stress into account for the evaluation of contact stress by the inverse analysis proposed by Weisz-Patrault et al. [4] on the other hand is demonstrated as follows. Hot rolling process is simulated by a 3D thermo-mechanical strip/roll stack coupled model proposed by Hacquin [10]. This model called Lam3/Tec3 is a software developed by Cemef, Transvalor, ArcelorMittal Research and Alcan, and it solves the strip elastic-viscoplastic strain by 3D FEM, and the roll stack elastic deformation by semi-analytical models.

Then the temperature field in the whole roll is computed by FDM by using Heat Transfer Coefficients (HTC). The rolling conditions are listed in Table 2. Among several authors, this model has been used by Legrand et al. [2], Weisz-Patrault et al. [4] and Abdelkhalek et al. [11] who gave more details on the formulation.

Many papers model rolling processes by FEM. For example Jiang and Tieu [12] proposed a 3D rigid plastic/visco-plastic FEM. More recently Montmitonnet [13] proposed a coupled numerical model for hot and cold rolling process. A comprehensive hot rolling process has also been modeled recently by Wang et al. [14]. Abdelkhalek et al. [11] used Lam3/Tec3 and added the computation of the post-bite buckling of the strip, in order to predict accurately flatness defects. Moreover Shahani et al. [15] simulated a hot rolling process of aluminum by FEM and used an artificial neural network in order to predict the behaviour of the strip during the rolling process (the artificial neural network being trained by the simulation). Lam3/Tec3 [10] has been chosen because the simulation was already done (directly taken from Legrand et al. [2]) and previously used for demonstrating the accuracy of the inverse method of Weisz-Patrault et al. [4]. Therefore the same simulation is used to demonstrate the exactness of the present thermal stress computation and the necessity of correcting the inputs of the inverse method of Weisz-Patrault et al. [4].

Among other outputs, Lam3/Tec3 [10] produces the contact stress (see Figure 7), then the temperature field inside the roll is computed (see Figure 3). The aim of the paper is not at simulating rolling process but at developing inverse analysis dedicated to measurement interpretation. These simulated contact stress and temperature field are only used as possible conditions for a work roll during hot rolling process for the only purpose of validating the presented method. Therefore the formulation of the model Lam3/Tec3 [10] is not reminded in this paper.

2.2. Validation of the analytical solution

The temperature field produced by the simulation of hot rolling process is used to compute the thermal stress with the analytical method developed in Sections 6 and 7. Moreover a simple linear and plain strain FE computation of the thermal stress has also been done with the freeware Cast3m [16] and a comparison (see Figure 5) is done to show the exactness of the present analytical solution. Very good agreement is obtained. It should be noted that this temperature field can be practically evaluated by using the analytical inverse analysis of Weisz-Patrault et al. [5] which interprets measurements of a thermocouple embedded inside the roll body. In this paper the temperature field is numerical but by considering the temperature at the radius R_c, the analytical form (14) is deduced (as it would have been done with real measurements).

2.3. Influence of thermal stress on contact stress reconstruction

Moreover the contact stress produced by Lam3/Tec3 [10] is used to compute the purely elastic stress inside the roll. The purely elastic stress tensor at the radius R_b corresponds with corrected inputs (free from thermal stress). The thermal stress at the radius R_b computed with the present method can also by added to the purely elastic stress to constitute thermo-elastic inputs (which replace measurements done with fibre optics). The evaluation of contact stress by using the inverse analysis proposed by Weisz-Patrault et al. [4] is done both with purely elastic inputs and thermo-elastic inputs and a comparison with the applied contact stress (produced by Lam3/Tec3 [10]) is proposed to show the necessity of taking the thermal stress into account for an accurate evaluation of contact stress.

3. Principle of superposition

The present method considers only the work roll. The strip is not modeled because this paper aims at developing inverse methods and not at simulating the rolling process with coupled FEM. The contact stress (mechanical boundary conditions) and temperature field are inferred from the inverse methods which interpret measurements of stress tensor and temperature at radii R_b and R_c.

The Figure 2 explains the decomposition of the problem. The auxiliary problem A is direct. The temperature field is considered as a thermal load. It is in the form of (14) introduced by Weisz-Patrault et al. [5] and briefly reminded in Section 5. The solution is only a particular solution, no specified boundary conditions are settled. Consequently the calculated tensile vector at the outer radius R_d (called $\boldsymbol{T}^A = \sigma^A_{rr}(R_d,\theta)\boldsymbol{e_r} + \sigma^A_{r\theta}(R_d,\theta)\boldsymbol{e_\theta}$) should be compensated by an other elastic problem with $-\boldsymbol{T}^A$ as boundary conditions. This is the purpose of the auxiliary problem B which is also direct (boundary conditions known). The superposition of both auxiliary problems A and B gives the thermal stress in the whole roll (considering that no displacement is blocked at the surface of the roll). Therefore $\sigma^{th} = \sigma^A + \sigma^B$, where *th* means thermal. All the notations are listed in Table 1

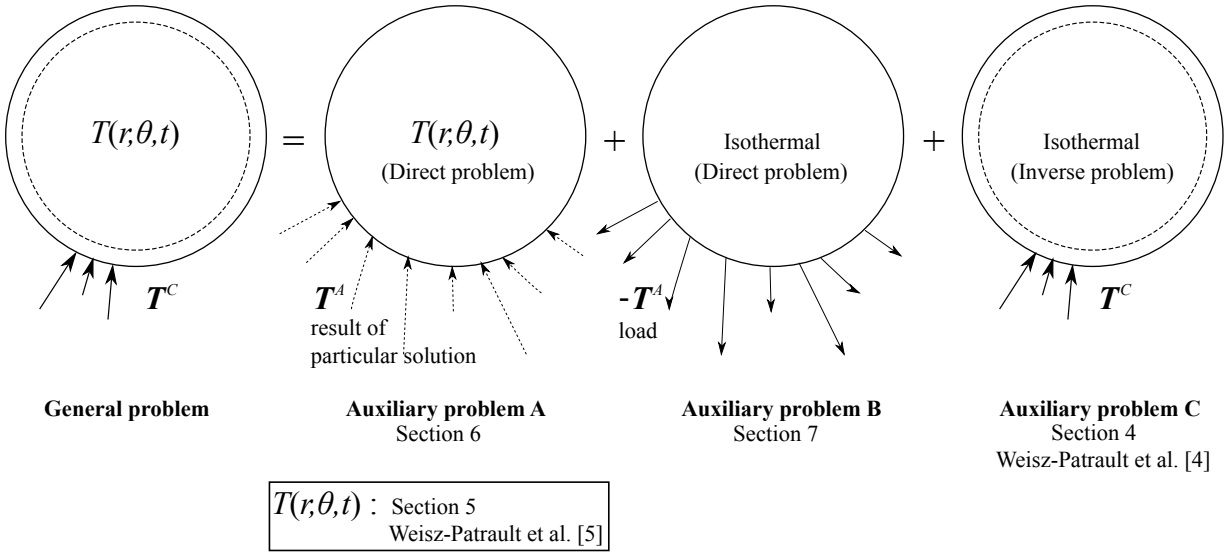

Figure 2: Superposition

4. Auxiliary problem C

This inverse problem has already been solved by Weisz-Patrault et al. [4]. However the basic principles of the solution are reminded in this section in order to make the reading easier. The fibre optics give the measurement of the stress tensor at the radius R_b called $\sigma^m_{rr}(\theta), \sigma^m_{r\theta}(\theta)$ and $\sigma^m_{\theta\theta}(\theta)$ where m means measured. Practically this stress tensor is measured with thermal stress, therefore $\sigma^m = \sigma^e + \sigma^{th}$ where e means purely elastic and th means thermal. This paper aims at determining σ^{th} which is done in Sections 6 and 7. The inputs of this inverse method are σ^e, which is determined simply by $\sigma^e = \sigma^m - \sigma^{th}$.

The elastic stress σ^C of the auxiliary problem C verifies the equations of elasticity for an isotropic material under the isothermal assumption given by Muskhelishvili [17]:

$$\left\{ \begin{array}{l} \sigma^C_{rr}(r,\theta) + \sigma^C_{\theta\theta}(r,\theta) = 2\left(f(z) + \overline{f(z)}\right) \\ -\sigma^C_{rr}(r,\theta) + \sigma^C_{\theta\theta}(r,\theta) + 2i\sigma^C_{r\theta}(r,\theta) = 2\exp(2i\theta)\left(g(z) + \overline{z}f'(z)\right) \end{array} \right. \tag{1}$$

where $z = r\exp(i\theta)$ and $f(z)$ and $g(z)$ are unknown holomorphic functions defined on the roll. Mathematically, these functions can be expanded into a power series. Therefore:

$$f(z) = \sum_{k=0}^{+\infty} f_k \left(\frac{z}{R_b}\right)^k \quad \left| \quad g(z) = \sum_{k=0}^{+\infty} g_k \left(\frac{z}{R_b}\right)^k \right. \tag{2}$$

By combining (1) and (2) and considering that $\sigma^C(R_b,\theta) = \sigma^e(\theta)$ it is obtained that:

$$\left\{ \begin{array}{l} \sigma^e_{rr}(\theta) + \sigma^e_{\theta\theta}(\theta) = 2\displaystyle\sum_{k=0}^{+\infty} f_k \exp(ik\theta) + \overline{f_k}\exp(-ik\theta) \\ -\sigma^e_{rr}(\theta) + \sigma^e_{\theta\theta}(\theta) + 2i\sigma^e_{r\theta}(\theta) = 2\displaystyle\sum_{k=0}^{+\infty} (g_k \exp(i(k+2)\theta) + kg_k \exp(ik\theta)) \end{array} \right. \tag{3}$$

By using (4), coefficients f_k and g_k are calculated by integrating the purely elastic part of the stresses measured at the inner radius (with fast fourier transform) using (5):

$$\int_{\partial C} z^k \, dz = \left\{ \begin{array}{ll} 2i\pi & k = -1 \\ 0 & k \neq -1 \end{array} \right. \tag{4}$$

$$\begin{cases} f_0 = \dfrac{1}{8\pi}\displaystyle\int_0^{2\pi} \sigma^e_{rr}(\theta) + \sigma^e_{\theta\theta}(\theta)\, d\theta \\ \\ \forall k \in \mathbb{N}^* \\ f_k = \dfrac{1}{4\pi}\displaystyle\int_0^{2\pi} \dfrac{\sigma^e_{rr}(\theta) + \sigma^e_{\theta\theta}(\theta)}{\exp(ik\theta)}\, d\theta \\ \\ \forall k \in \mathbb{N} \\ g_k = \dfrac{1}{4\pi}\displaystyle\int_0^{2\pi} \dfrac{-\sigma^e_{rr}(\theta) + \sigma^e_{\theta\theta}(\theta) + 2i\sigma^e_{r\theta}(\theta)}{\exp(i(k+2)\theta)}\, d\theta - (k+2) f_{k+2} \end{cases} \tag{5}$$

By combining (1) and (2), the stresses in the roll gap as a function of f_k and g_k are obtained:

$$\begin{cases} \sigma^C_{rr}(R_d,\theta) + \sigma^C_{\theta\theta}(R_d,\theta) = 2\displaystyle\sum_{k=0}^{+\infty}\left(\frac{R_d}{R_b}\right)^k (f_k \exp(ik\theta) + \overline{f_k}\exp(-ik\theta)) \\ -\sigma^C_{rr}(R_d,\theta) + \sigma^C_{\theta\theta}(R_d,\theta) + 2i\sigma^C_{r\theta}(R_d,\theta) = 2\displaystyle\sum_{k=0}^{+\infty}\left(\frac{R_d}{R_b}\right)^k (g_k \exp(i(k+2)\theta) + k f_k \exp(ik\theta)) \end{cases} \tag{6}$$

By eliminating $\sigma^C_{\theta\theta}(R_d,\theta)$ in (6) the contact tensile vector $\boldsymbol{T}^C = \sigma^C_{rr}(R_d,\theta)\boldsymbol{e_r} + \sigma^C_{r\theta}(R_d,\theta)\boldsymbol{e_\theta}$ is easily found.

5. Analytical temperature field

This inverse problem has already been solved by Weisz-Patrault et al. [5]. However the basic principles of the solution are reminded in this section in order to make the reading easier. The temperature is measured at the radius R_c and is called $T^m(\theta)$. The linear heat equation for a rotating body is:

$$\frac{\partial^2 T}{\partial r^2} + \frac{1}{r}\frac{\partial T}{\partial r} + \frac{1}{r^2}\frac{\partial^2 T}{\partial \theta^2} = \frac{1}{D}\left(\frac{\partial T}{\partial t} + \omega\frac{\partial T}{\partial \theta}\right) \tag{7}$$

where D is the thermal diffusivity (assumed to be constant).

Two families of analytical solutions of (7) are used. The solution (8) is steady and solution (9) is transient:

$$\gamma J_n\left(\sqrt{-\frac{i\omega n}{D}}r\right)\exp(in\theta) \tag{8}$$

$$\gamma J_0\left(\sqrt{\frac{1}{D\tau}}r\right)\exp\left(-\frac{t}{\tau}\right) \tag{9}$$

The solution is written as a linear combination of these families of solutions (8) and (9). The solution is divided into two parts: T_1 which is the steady solution (updated at each cycle) and T_2 which is the transient solution. The measured temperature is expanded into a Fourier series:

$$T^m(\theta) = \sum_{n=-N_1}^{N_1} T_n \exp(in\theta) \tag{10}$$

where the Fourier coefficients (11) can be computed from measurements with fft:

$$T_n = \frac{1}{2\pi}\int_0^{2\pi} T^m(\theta)\exp(-in\theta)\, d\theta \tag{11}$$

Therefore if $\zeta_n = \sqrt{-i\omega n/D}$ then T_1 defined by (12) is a solution in the form of (8) and matches the measurements at $r = R_c$.

$$T_1(r,\theta) = \sum_{n=-N_1}^{N_1} T_n \frac{J_n(\zeta_n r)}{J_n(\zeta_n R_c)}\exp(in\theta) \tag{12}$$

It is demonstrated by Weisz-Patrault et al. [5] that if x_n are the successive positive zeros of the Bessel function of the order zero, then the function given by (13) is a solution of (7) in the form of (9) which vanishes at $r = R_c$ and

is a very good approximation in order to verify the initial condition (at $t = 0$ the temperature in the whole roll is the room temperature):

$$T_2(r,t) = \sum_{n=1}^{N_2} \gamma_n J_0\left(x_n \frac{r}{R_c}\right) \exp\left(-x_n^2 \frac{Dt}{R_c^2}\right) \tag{13}$$

where the coefficients γ_n are evaluated by using the detailed method presented by Weisz-Patrault et al. [5]. The complete solution is therefore:

$$T(r,\theta,t) = \sum_{n=-N_1}^{N_1} T_n \frac{J_n(\zeta_n r)}{J_n(\zeta_n R_c)} \exp(in\theta) + \sum_{n=1}^{N_2} \gamma_n J_0\left(x_n \frac{r}{R_c}\right) \exp\left(-x_n^2 \frac{Dt}{R_c^2}\right) \tag{14}$$

6. Auxiliary problem A

The auxiliary problem A defined in Figure 2 is a direct quasi-static problem of elasticity with a right hand term corresponding to the temperature field, which is known in the whole roll in the form of (14). The mechanical boundary conditions are not specified because only a particular solution is sought. The calculated tensile vector at the outer radius $\boldsymbol{T}^A$ will be compensated by an isothermal elastic problem with $-\boldsymbol{T}^A$ as boundary conditions (auxiliary problem B).

6.1. Displacements

For an isotropic medium the Navier's equation with a right hand term is used:

$$\mu \text{div grad } \boldsymbol{u} + (\lambda+\mu)\text{grad div } \boldsymbol{u} = \alpha(3\lambda+2\mu)\text{grad } T \tag{15}$$

By writing $\boldsymbol{u}$ in polar coordinates the following differential equations system is obtained:

$$\begin{cases} (\lambda+2\mu)\left(\dfrac{\partial^2 u_r}{\partial r^2} + \dfrac{1}{r}\dfrac{\partial u_r}{\partial r} - \dfrac{u_r}{r^2}\right) + \mu\dfrac{1}{r^2}\dfrac{\partial^2 u_r}{\partial \theta^2} + (\lambda+\mu)\dfrac{1}{r}\dfrac{\partial^2 u_\theta}{\partial r \partial \theta} - (\lambda+3\mu)\dfrac{1}{r^2}\dfrac{\partial u_\theta}{\partial \theta} = \alpha(3\lambda+2\mu)\dfrac{\partial T}{\partial r} \\ \mu\left(\dfrac{\partial^2 u_\theta}{\partial r^2} + \dfrac{1}{r}\dfrac{\partial u_\theta}{\partial r} - \dfrac{u_\theta}{r^2}\right) + (\lambda+2\mu)\dfrac{1}{r^2}\dfrac{\partial^2 u_\theta}{\partial \theta^2} + (\lambda+\mu)\dfrac{1}{r}\dfrac{\partial^2 u_r}{\partial r \partial \theta} + (\lambda+3\mu)\dfrac{1}{r^2}\dfrac{\partial u_r}{\partial \theta} = \alpha(3\lambda+2\mu)\dfrac{1}{r}\dfrac{\partial T}{\partial \theta} \end{cases} \tag{16}$$

The temperature field is known and can be written in the form of (14), therefore the polar displacements u_r and u_θ are sought in the form:

$$\begin{cases} u_r(r,\theta) = \displaystyle\sum_{n=1}^{N_1}\left(P_n(r)\exp(in\theta) + \overline{P_n}(r)\exp(-in\theta)\right) + \sum_{n=1}^{N_2} p_n(r)\exp\left(-x_n^2\frac{Dt}{R_c^2}\right) \\ u_\theta(r,\theta) = \displaystyle\sum_{n=1}^{N_1}\left(Q_n(r)\exp(in\theta) + \overline{Q_n}(r)\exp(-in\theta)\right) + \sum_{n=1}^{N_2} q_n(r)\exp\left(-x_n^2\frac{Dt}{R_c^2}\right) \end{cases} \tag{17}$$

For convenience the following quantities are introduced:

$$\begin{cases} L_n = \alpha\left(\dfrac{3\lambda+2\mu}{\lambda+2\mu}\right)\left(\dfrac{\zeta_n T_n}{J_n(\zeta_n R_c)}\right) \\ l_n = \alpha\left(\dfrac{3\lambda+2\mu}{\lambda+2\mu}\right)\left(\dfrac{\gamma_n R_c}{x_n}\right) \end{cases} \tag{18}$$

It should be noted that the quantities $\{P_n(r), Q_n(r), p_n(r), q_n(r), L_n, l_n\}$ are updated at each cycle, but subscripts of cycles are omitted to make the reading easier. The system (16) combined with (17) and (18) gives:

$$\begin{cases} (\lambda+2\mu)\left(P_n''(r)+\dfrac{P_n'(r)}{r}-\dfrac{P_n(r)}{r^2}\right)-\mu n^2\dfrac{P_n(r)}{r^2}+(\lambda+\mu)in\dfrac{Q_n'(r)}{r}-(\lambda+3\mu)in\dfrac{Q_n(r)}{r^2}=(\lambda+2\mu)L_nJ_n'(\zeta_n r) \\ \mu\left(Q_n''(r)+\dfrac{Q_n'(r)}{r}-\dfrac{Q_n(r)}{r^2}\right)-(\lambda+2\mu)n^2\dfrac{Q_n(r)}{r^2}+(\lambda+\mu)in\dfrac{P_n'(r)}{r}+(\lambda+3\mu)in\dfrac{P_n(r)}{r^2}=in(\lambda+2\mu)L_n\dfrac{J_n(\zeta_n r)}{\zeta_n r} \\ p_n''(r)+\dfrac{p_n'(r)}{r}-\dfrac{p_n(r)}{r^2}=l_n\left(\dfrac{x_n}{R_c}\right)^2J_0'\left(x_n\dfrac{r}{R_c}\right) \\ q_n''(r)+\dfrac{q_n'(r)}{r}-\dfrac{q_n(r)}{r^2}=0 \end{cases} \tag{19}$$

A particular solution of (19) is given by (proof appended in Appendix A):

$$\forall n\geq 1 \quad \begin{cases} P_n(r)=-\dfrac{L_n}{\zeta_n^2}J_n'(\zeta_n r) \\ Q_n(r)=-in\dfrac{L_n}{\zeta_n^2}\dfrac{J_n(\zeta_n r)}{\zeta_n r} \end{cases} \tag{20}$$

$$\forall n\geq 1 \quad \begin{cases} p_n(r)=-l_nJ_0'\left(x_n\dfrac{r}{R_c}\right) \\ q_n(r)=0 \end{cases}$$

Therefore the displacement field has been solved by plugging (20) in (17).

6.2. Stress

By using an isotropic behavior of the medium the following system is obtained:

$$\begin{cases} \sigma_{rr}^A=(\lambda+2\mu)\dfrac{\partial u_r}{\partial r}+\lambda\left(\dfrac{u_r}{r}+\dfrac{1}{r}\dfrac{\partial u_\theta}{\partial\theta}\right)-\alpha(3\lambda+2\mu)\left(T(r,\theta,t)-T_a\right) \\ \sigma_{r\theta}^A=\mu\left(\dfrac{1}{r}\dfrac{\partial u_r}{\partial\theta}+\dfrac{\partial u_\theta}{\partial r}-\dfrac{u_\theta}{r}\right) \\ \sigma_{\theta\theta}^A=\lambda\dfrac{\partial u_r}{\partial r}+(\lambda+2\mu)\left(\dfrac{u_r}{r}+\dfrac{1}{r}\dfrac{\partial u_\theta}{\partial\theta}\right)-\alpha(3\lambda+2\mu)\left(T(r,\theta,t)-T_a\right) \end{cases} \tag{21}$$

Therefore by using (21) and (17) the stress tensor is expressed:

$$\sigma_{\cdot\cdot}^A(r,\theta)=\sum_{n=1}^{N_1}\left(S_{\cdot\ddot{n}}(r)\exp(in\theta)+\overline{S_{\cdot\ddot{n}}}(r)\exp(-in\theta)\right)+S_{\cdot\ddot{0}}+\sum_{n=1}^{N_2}s_{\cdot\ddot{n}}(r)\exp\left(-x_n^2\frac{Dt}{R_c^2}\right) \tag{22}$$

where (..) can be replaced by rr, $r\theta$ or $\theta\theta$ and:

$$\begin{cases} S_0^{rr}(r) = \alpha(3\lambda + 2\mu)(T_a - T_0) \\ S_0^{r\theta}(r) = 0 \\ S_0^{\theta\theta}(r) = \alpha(3\lambda + 2\mu)(T_a - T_0) \end{cases}$$

$$\forall n \geq 1 \quad \begin{cases} S_n^{rr}(r) = \dfrac{2\mu L_n}{\zeta_n}\left(\dfrac{J_n'(\zeta_n r)}{\zeta_n r} - n^2\dfrac{J_n(\zeta_n r)}{\zeta_n^2 r^2}\right) \\ S_n^{r\theta}(r) = \dfrac{2\mu i n L_n}{\zeta_n}\left(-\dfrac{J_n'(\zeta_n r)}{\zeta_n r} + \dfrac{J_n(\zeta_n r)}{\zeta_n^2 r^2}\right) \\ S_n^{\theta\theta}(r) = -\dfrac{2\mu L_n}{\zeta_n}\left(\dfrac{J_n'(\zeta_n r)}{\zeta_n r} - \left(\dfrac{n^2}{\zeta_n^2 r^2} - 1\right)J_n(\zeta_n r)\right) \end{cases} \tag{23}$$

$$\forall n \geq 1 \quad \begin{cases} s_n^{rr}(r) = \dfrac{2\mu l_n}{r} J_0'\left(\dfrac{x_n r}{R_c}\right) \\ s_n^{r\theta}(r) = 0 \\ s_n^{\theta\theta}(r) = -\dfrac{2\mu l_n x_n}{R_c}\left(J_0'\left(\dfrac{x_n r}{R_c}\right)\dfrac{R_c}{x_n r} + J_0\left(\dfrac{x_n r}{R_c}\right)\right) \end{cases}$$

7. Auxiliary problem B

The Figure 2 shows that the plane elastic problem B is isothermal. Therefore the complex equations system given by Muskhelishvili [17] is used:

$$\begin{cases} \sigma_{rr}^B(r,\theta) + \sigma_{\theta\theta}^B(r,\theta) = 2\left(\Phi(z) + \overline{\Phi(z)}\right) \\ -\sigma_{rr}^B(r,\theta) + \sigma_{\theta\theta}^B(r,\theta) + 2i\sigma_{r\theta}^B(r,\theta) = 2\exp(2i\theta)\left(\Psi(z) + \overline{z}\Phi'(z)\right) \end{cases} \tag{24}$$

where $z = r\exp(i\theta)$ (with (r,θ) the position where the stress is calculated) and $\Phi(z)$ and $\Psi(z)$ are two unknown holomorphic functions. Mathematically, these functions can be expanded into a power series. Therefore:

$$\Phi(z) = \sum_{n=0}^{N_1} \phi_k z^k \quad \Big| \quad \Psi(z) = \sum_{n=0}^{N_1} \psi_k z^k \tag{25}$$

The opposite tensile vector calculated for the auxiliary problem A (given in Section 6) is applied.

$$\boldsymbol{T}^B = -\boldsymbol{T}^A = -\sigma_{rr}^A(R_d,\theta)\boldsymbol{e_r} - \sigma_{r\theta}^A(R_d,\theta)\boldsymbol{e_\theta} \tag{26}$$

By rewriting (24) at the boundary (i.e., for $z = R_d\exp(i\theta)$) and by subtracting both equations:

$$-\sigma_{rr}^A(R_d,\theta) + i\sigma_{r\theta}^A(R_d,\theta) = \Phi(z) - \frac{z^2}{R_d^2}\Psi(z) - z\Phi'(z) + \overline{\Phi(z)} \tag{27}$$

By combining (27) and (25), the stresses in the roll gap as a function of ϕ_k and ψ_k are obtained:

$$-\sigma_{rr}^A(R_d,\theta) + i\sigma_{r\theta}^A(R_d,\theta) = \sum_{n=2}^{N_1}\left(\phi_n(1-n)R_d^n - \psi_{n-2}R_d^{n-2}\right)\exp(in\theta) + \sum_{n=1}^{N_1}\overline{\phi_n}\exp(-in\theta) + \phi_0 + \overline{\phi_0} \tag{28}$$

By injecting (22) into (28):

$$\begin{cases} \phi_0 + \overline{\phi_0} = -S_0^{rr}(R_d) - \displaystyle\sum_{n=0}^{N_2} s_n^{rr}(R_d)\exp\left(-x_n^2\frac{Dt}{R_c^2}\right) & \\ \phi_n = -\dfrac{S_n^{rr}(R_d) + iS_n^{r\theta}(R_d)}{R_d^n} & (\forall n \geq 1) \\ \psi_{n-2} = \dfrac{nS_n^{rr}(R_d) - i(2-n)S_n^{r\theta}(R_d)}{R_d^{n-2}} & (\forall n \geq 2) \end{cases} \tag{29}$$

The equation (24) can be rewritten:

$$\begin{cases} \sigma^B_{rr}(r,\theta) + \sigma^B_{\theta\theta}(r,\theta) = 2\sum_{k=0}^{N_1} r^k(\phi_k \exp(ik\theta) + \overline{\phi_k}\exp(-ik\theta)) \\ -\sigma^B_{rr}(r,\theta) + \sigma^B_{\theta\theta}(r,\theta) + 2i\sigma^B_{r\theta}(r,\theta) = 2\sum_{k=0}^{N_1} r^k(\psi_k \exp(i(k+2)\theta) + k\phi_k \exp(ik\theta)) \end{cases} \tag{30}$$

It is fairly easy to derive $\sigma^B_{rr}(r,\theta)$, $\sigma^B_{r\theta}(r,\theta)$ and $\sigma^B_{\theta\theta}(r,\theta)$ by taking the sum and the difference of both equations of (30).

Finally, the thermal stress is defined by:

$$\sigma^{th}_{..} = \sigma^A_{..} + \sigma^B_{..} \tag{31}$$

where (..) can be replaced by rr, $r\theta$ or $\theta\theta$.

8. Validation of the solution

8.1. Temperature field

The temperature field in the whole roll is extracted from the simulation of the hot rolling process presented in Section 2. By considering the temperature at the radius R_c the Fourier coefficients (11) are computed and the temperature field is expressed in the form of (14) and is given in Figure 3 at radii R_c and R_d. It should be noted that the temperature field is consistent with typical temperature fields that occur during hot rolling processes as observed by Corral et al. [6] or more recently Abbaspour and Saboonchi [18]. The Fourier coefficients T_n computed from the temperatures at the radius R_c by using (11) are listed in Table B.4 and the coefficients γ_n are listed in Table B.5 (appended in Appendix B). The rolling parameters are listed in Table 2.

Table 2: Parameters

(a) Roll

R_d	(mm)	177.51
R_c	(mm)	177.01
R_b	(mm)	174.51
T_a	(K)	293.15
D	(mm^2/s)	13.5
α	(K^{-1})	12×10^{-6}
λ	(MPa)	121153.85
μ	(MPa)	80769.231
ω	(rad/s)	18.76

(b) Strip

Material		Steel
t_i	(mm)	56.2
t_f	(mm)	31.2
R	(%)	44.48
F_R	(N/mm)	8867
σ_0	(MPa)	150
T_i	(K)	1275.15
HTC	($W/m^2/K$)	70000
L_c	(mm)	70

(c) Solution

N_1	200
N_2	60

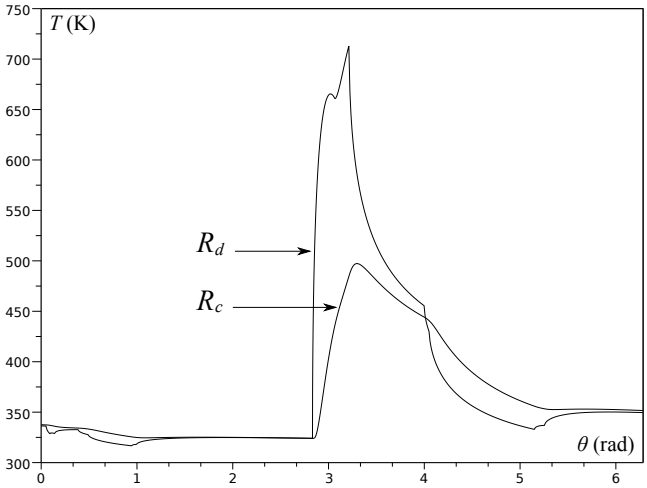

Figure 3: Temperature for hot rolling conditions at the radii R_d and R_c.

8.2. Comparison with FEM

The thermal stress of the present analytical method is obtained by adding the solutions of the auxiliary problem A in Section.6 and the auxiliary problem B in Section.7, therefore $\sigma^{th} = \sigma^{A} + \sigma^{B}$ (the superscript *th* meaning thermal). This thermal stress is validated by comparing the method presented in this paper and a numerical model by FEM performed with the freeware Cast3m developed by CEA [16]. The temperature field presented in Section 8.1 is used for the computation. Considering the extremely sharp gradients near the surface of the roll, the mesh is refined in this area. The mesh is generated by rotating (200 increments) a line defined by 10 nodes from the center to 167.51 mm and 100 nodes from 167.51 mm to 177.51 mm. Triangular elements are chosen. The figure 4 shows the final mesh. The computation with Cast3m is linear and plane strain. The temperature is specified at each node of the mesh, and the equilibrium is ensured by blocking the central node. The comparison is presented in Figure 5, and a good agreement is observed. The exactness of the analytical thermal stress presented in Sections 6 and 7 is verified.

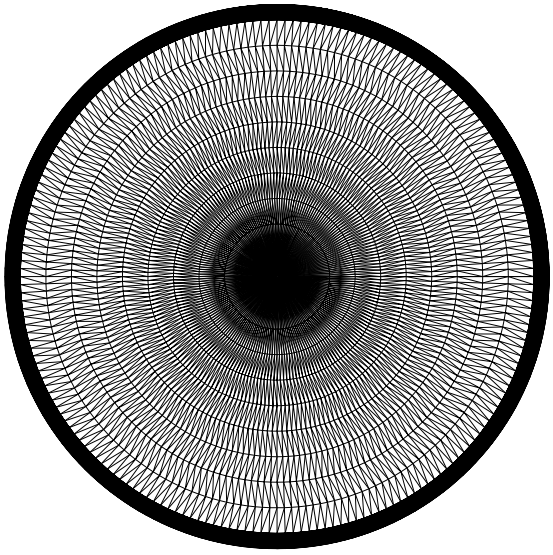

Figure 4: Mesh for comparison with FEM (Cast3m)

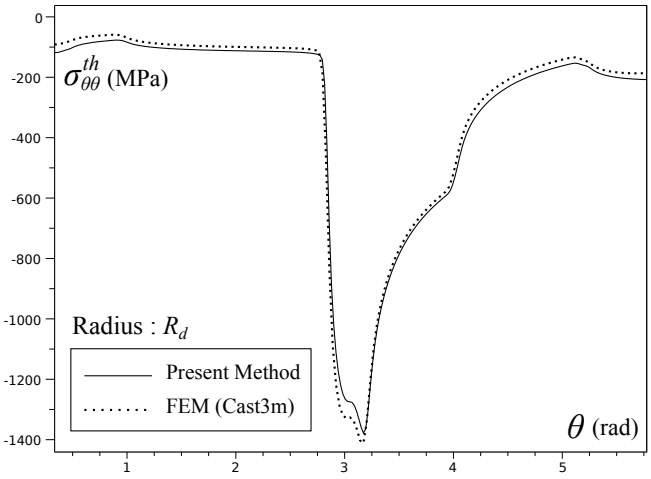

Figure 5: Comparison of thermal stress with FEM (Cast3m)

8.3. Comparison with other analytical models

Corral et al. [6] used an analytical solution of the Navier's Equation (15), by simplifying the problem by neglecting the rotation terms and decoupling the radial displacement and the tangential displacement. The analytical formula given by the authors is used with the temperature field described in Section 8.1. The Figure 6 shows that the thermal stress $\sigma^{th}_{\theta\theta}$ at the outer radius R_d is underestimated by Corral et al. [6]. The present analytical solution is therefore an improvement which can be used as inputs of other models (thermal fatigue for instance).

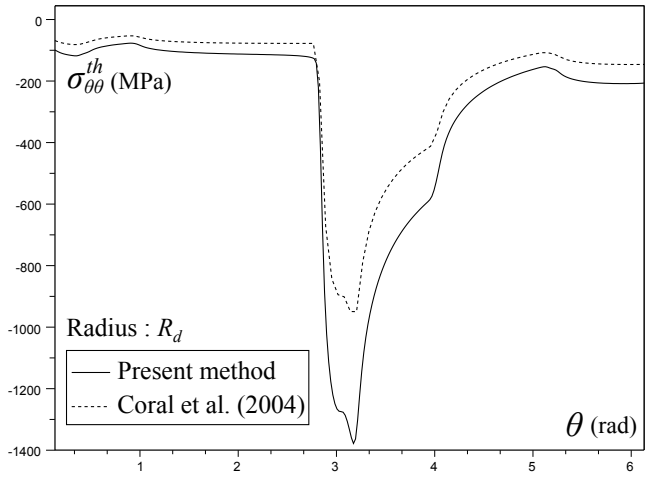

Figure 6: Comparison of thermal stress with other analytical model

9. Reconstructed stress comparison

As explained in Section 2 a numerical simulation of hot rolling process is done with Lam3/Tec3 [10]. The industrial hot rolling conditions chosen for the simulation are taken from Legrand et al. [2] and are listed in Table 2. The impact of the thermal stress on the reconstruction of the contact stress by inverse analysis is evaluated in this section. The purely elastic contact stress profiles at the outer radius R_d for normal pressure (σ_{rr}) and shear stress ($\sigma_{r\theta}$) are given in Figure 7.

The inputs of the inverse method proposed by Weisz-Patrault et al. [4] are the stresses at the radius R_b. In order to quantify the impact of thermal stress and the necessity of correction, two kinds of inputs are distinguished: the thermoelastic stresses (which simulate the measurements of fibre optics) and the purely elastic stresses, which can be practically deduced from the measurements of the fibre optics by using the present method and removing the thermal stress.

Therefore the thermal stress calculated at the radius R_b is added to the purely elastic stress also calculated at the inner radius R_b. These stress distributions are given in Figure 8. The hoop stress $\sigma_{\theta\theta}$ is clearly the most affected by the thermal dilatation of the roll. It can be noted that the difference between the thermoelastic hoop stress and the purely elastic hoop stress is relatively constant. This is the consequence of the diffusion of the temperature into the roll. R_b is at 3 mm from the surface, at this depth the thermal hoop stress varies slightly compared to the variations observed at the radius R_d (surface of the roll). Moreover the area around the roll gap being small, the variations of thermal stresses are quite small as shown in Figure 9.

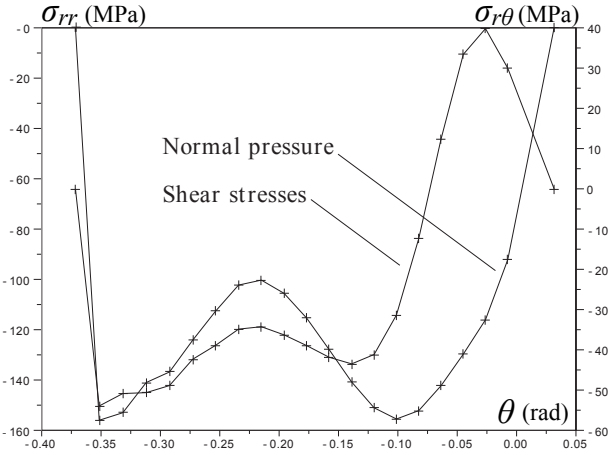

Figure 7: Purely elastic contact stresses at radius R_d

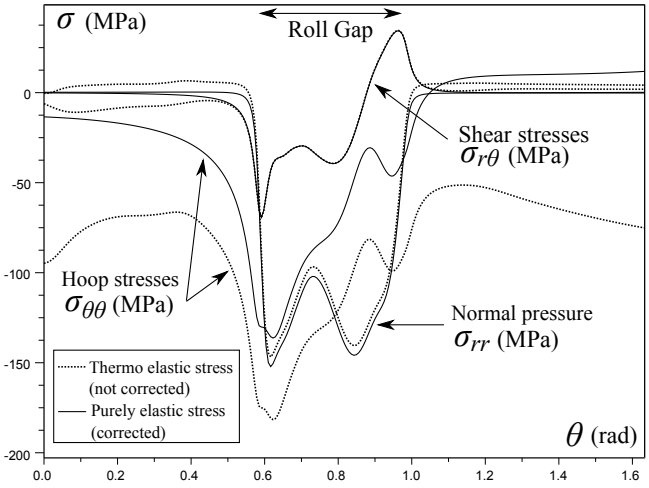

Figure 8: Stress tensor calculated at R_b

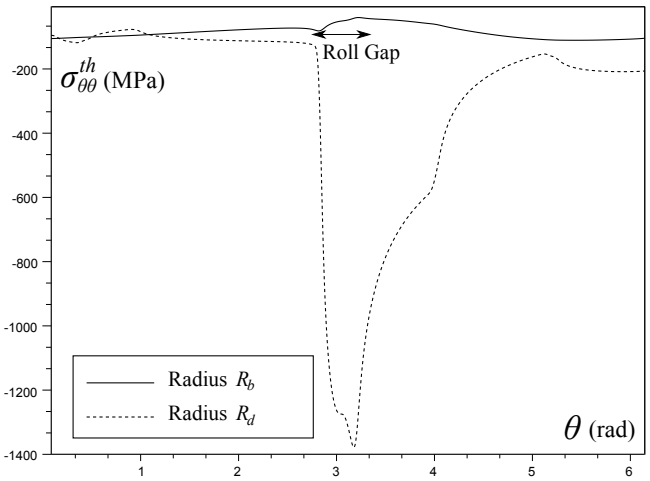

Figure 9: Thermal hoop stress at radii R_b and R_d

The inverse calculation proposed by Weisz-Patrault et al. [4] is performed both for purely elastic inputs (corrected data) and thermoelastic inputs (not corrected data) and the results (contact stress in the roll gap) are presented in Figures 10 and 11. In order to quantify the error between the applied stress and the reconstructed stress an error estimate is introduced in (32). If σ^r and σ^a denote respectively the reconstructed stress and the applied stress:

$$\epsilon = \sqrt{\frac{\int_0^{2\pi} (\sigma^r(\theta) - \sigma^a(\theta))^2 \, d\theta}{\int_0^{2\pi} \sigma^a(\theta)^2 \, d\theta}} \tag{32}$$

The Table 3 lists the quantified errors of reconstruction. The improvement of the reconstruction with corrected data with the present thermoelastic method is very significant. The correction of the inputs is therefore necessary to perform accurately the inverse method proposed by Weisz-Patrault et al. [4].

Table 3: Hot rolling summary

	Purely elastic inputs (corrected)		Thermoelastic inputs (not corrected)	
	rr	$r\theta$	rr	$r\theta$
ϵ (%)	0.63	0.75	25.41	17.75

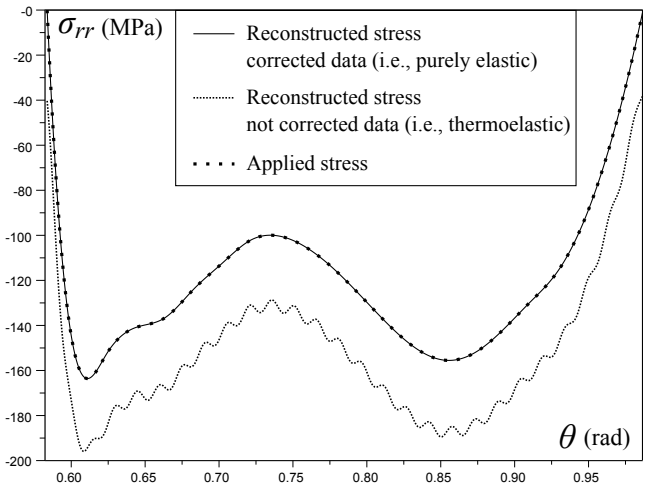

Figure 10: Reconstructed normal pressure σ_{rr} at the outer radius R_d

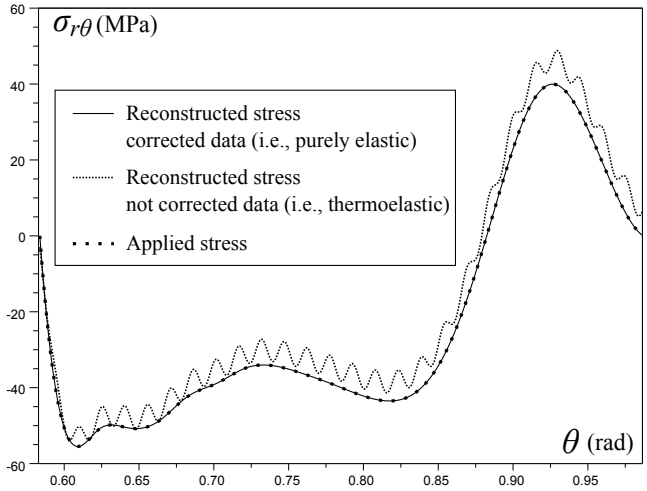

Figure 11: Reconstructed shear stress $\sigma_{r\theta}$ at the outer radius R_d

10. Computation time

The computation time is studied to rapidly optimise the industrial parameters during the rolling process. The principle is to write the solution in matrix form. The matrices can be computed off-line (i.e., before the rolling process) and be stocked in a library. Let N_θ be the number of angular positions θ_j (j varying from 1 to N_θ) where the outputs are computed. The CPU times of the inverse methods proposed by Weisz-Patrault et al. [4] and Weisz-Patrault et al. [5] are optimised (CPU times displayed by Scilab 5.3 are respectively 0.07 s and 0.05 s with a quadcore 2.8 GHz). Therefore the following optimisation is only about the thermal stress $\sigma^{th} = \sigma^A + \sigma^B$ which is written as follows ((..) replaces rr, $r\theta$ or $\theta\theta$):

$$\sigma^A_{\cdot\cdot}(\theta, t_0) = 2\mathrm{Re}\left(A^{\cdot\cdot}.\boldsymbol{L}\right) + S^{\cdot\cdot}_0 + \boldsymbol{a}^{\cdot\cdot}.\boldsymbol{l} \tag{33}$$

where the matrices $A^{(rr)}$, $A^{(r\theta)}$ and $A^{(\theta\theta)}$ (size $N_\theta \times N_1$) are:

$$\left\{\begin{array}{l} A^{rr}_{j,n} = \dfrac{2\mu}{\zeta_n}\left(\dfrac{J'_n(\zeta_n r)}{\zeta_n r} - n^2\dfrac{J_n(\zeta_n r)}{\zeta_n^2 r^2}\right)\exp\left(in\theta_j\right) \\ A^{r\theta}_{j,n} = \dfrac{2\mu in}{\zeta_n}\left(-\dfrac{J'_n(\zeta_n r)}{\zeta_n r} + \dfrac{J_n(\zeta_n r)}{\zeta_n^2 r^2}\right)\exp\left(in\theta_j\right) \\ A^{\theta\theta}_{j,n} = -\dfrac{2\mu}{\zeta_n}\left(\dfrac{J'_n(\zeta_n r)}{\zeta_n r} - \left(\dfrac{n^2}{\zeta_n^2 r^2} - 1\right)J_n(\zeta_n r)\right)\exp\left(in\theta_j\right) \end{array}\right. \tag{34}$$

where the vectors $\boldsymbol{a}^{rr}$, $\boldsymbol{a}^{r\theta}$ and $\boldsymbol{a}^{\theta\theta}$ (size $N_2 + 1$) are:

$$\left\{\begin{array}{l} a^{rr}_n = \dfrac{2\mu}{r}J'_0\left(\dfrac{x_n r}{R_c}\right)\exp\left(-x_n^2\dfrac{D}{R_c^2}t_0\right) \\ a^{r\theta}_n = 0 \\ a^{\theta\theta}_n = -\dfrac{2\mu x_n}{R_c}\left(J'_0\left(\dfrac{x_n r}{R_c}\right)\dfrac{R_c}{x_n r} + J_0\left(\dfrac{x_n r}{R_c}\right)\right)\exp\left(-x_n^2\dfrac{D}{R_c^2}t_0\right) \end{array}\right. \tag{35}$$

where the vector $\boldsymbol{L}$ (size N_1) is the vector of the L_n, and the vector $\boldsymbol{l}$ (size $N_2 + 1$) is the vector of the l_n.

$$\left\{\begin{array}{l} \sigma^B_{rr} + \sigma^B_{\theta\theta} = 2\mathrm{Re}\left(B_1.\boldsymbol{\phi}\right) \\ -\sigma^B_{rr} + \sigma^B_{\theta\theta} + 2i\sigma^B_{r\theta} = B_2.\boldsymbol{\psi} + B_3.\boldsymbol{\phi} \end{array}\right. \tag{36}$$

where the matrices B_1, B_2 and B_3 (size $N_\theta \times N_1$) are:

$$\left\{\begin{array}{l} B_{1\cdot j,n} = 2\left(\dfrac{R_b}{R_d}\right)^n\exp\left(in\theta_j\right) \\ B_{2\cdot j,n} = 2\left(\dfrac{R_b}{R_d}\right)^n\exp\left(i(n+2)\theta_j\right) \\ B_{3\cdot j,n} = 2\left(\dfrac{R_b}{R_d}\right)^n n\exp\left(in\theta_j\right) \end{array}\right. \tag{37}$$

and where $\boldsymbol{\phi}$ is the vector of ϕ_k and $\boldsymbol{\psi}$ is the vector of ψ_k.

The matrices $A^{(rr)}$, $A^{(r\theta)}$, $A^{(\theta\theta)}$,B_1, B_2 and B_3 and the vectors $\boldsymbol{a}^{rr}$, $\boldsymbol{a}^{r\theta}$ and $\boldsymbol{a}^{\theta\theta}$ are computed off-line (i.e., before the rolling process) and stocked in a library. $\boldsymbol{L}$, $\boldsymbol{l}$, $\boldsymbol{\phi}$ and $\boldsymbol{\psi}$ are computed on-line because the measured temperatures and the measured stresses are needed. However, these quantities are already computed because both inverse methods proposed by Weisz-Patrault et al. [4] and Weisz-Patrault et al. [5] are using them. Therefore the correction of the input data (thermoelastic stress giving purely elastic stress) does not cost significant additional CPU times (only the matrices products which is negligible). This is one of the main advantage of this analytical solution.

11. Conclusions

A successful method has been presented to compute the thermal stress during hot rolling on the basis of temperature fields expanded into series. These temperature fields are produced by an inverse analysis which interprets temperature measurements (thermocouple fully embedded in the roll). This problem is mainly used in this contribution to correct the inputs of an other inverse analysis which interprets stress measurements (fibre optics fully embedded in the roll) to compute the contact stress in the roll gap. The purely elastic stress is inferred from the measured (or simulated) thermoelastic stress by using the presented analytical method. It is demonstrated that this correction is necessary, the error being significantly reduced (from 25.41 % to 0.63 % for normal pressures and from 17.75 % to 0.75 % for shear stresses).

Both inverse methods proposed by Weisz-Patrault et al. [4] and Weisz-Patrault et al. [5] are designed for real time computation. The main advantage of the present correction is that it does not cost additional CPU times (or negligible: matrices products).

Moreover, the computation of thermal stress is more accurate than older analytical methods, and therefore can be used in the field of thermal fatigue of rolls both experimentally (measurement interpretation) and theoretically (simulations).

References

[1] P. Montmitonnet, A. Stephany, S. Cassarini, J. Ponthot, M. Laugier, N. Legrand, Modeling of metal forming lubrication by o/w emulsions, in: Int. Conf. Trib. Mat. Proc., Yokohama, pp. 85–90.

[2] N. Legrand, T. Lavalard, A. Martins, New concept of friction sensor for strip rolling: Theoretical analysis, Wear (2011) –.

[3] D. Meierhofer, K. Stelson, Measurement of the interfacial streses in rolling using the elastic deformation of the roll, Journal of engineering for industry 109 (1987) 362–369.

[4] D. Weisz-Patrault, A. Ehralcher, N. Legrand, A new sensor for the evaluation of contact stress by inverse analysis during steel strip rolling, Journal of Materials Processing Technology 211 (2011) 1500–1509.

[5] D. Weisz-Patrault, A. Ehralcher, N. Legrand, Evaluation of temperature field and heat flux by inverse analysis during steel strip rolling, International Journal of Heat and Mass Transfer 55 (2012) 629–641.

[6] R. Corral, R. Colas, A. Perez, Modeling the thermal and thermoelastic responses of work rolls used for hot rolling steel strip, Journal of Materials Processing Technology 153 (2004) 886–893.

[7] C.-S. Li, H.-L. Yu, G.-Y. Deng, X.-H. Liu, G.-D. Wang, Numerical simulation of temperature field and thermal stress field of work roll during hot strip rolling, Journal of Iron and Steel Research International 14 (2007) 18–21.

[8] D. Weisz-Patrault, A. Ehralcher, N. Legrand, N. Labbe, J. Horsky, T. Luks, Experimental study of interfacial heat flux and surface temperature by inverse analysis with thermocouple (fully embedded) during hot steel strip rolling, Advanced Materials Research 452-453 (2012) 959–953.

[9] N. Legrand, N. Labbe, D. Weisz-Patrault, A. Ehralcher, J. Horsky, T. Luks, Analysis of roll gap heat transfers in hot steel strip rolling through roll temperature sensors and heat transfer models, Key Engineering Materials 504-506 (2012) 1043–1048.

[10] A. Hacquin, Modelisation thermo-mecanique tridimensionnelle du laminage: couplage bande-cylindres (3D thermomechanical modelling of rolling processes: coupling strip and rolls), Ph.D. thesis, Cemef Ecole des Mines de Paris, 1996. In French.

[11] S. Abdelkhalek, P. Montmitonnet, N. Legrand, P. Buessler, Coupled approach for flatness prediction in cold rolling of thin strip, International Journal of Mechanical Sciences 53 (2011) 661–675.

[12] Z. Jiang, A. Tieu, Modeling of the rolling processes by a 3-D rigid plastic/ visco-plastic finite element method with shifted ICCG method, Comput Struct 40 (2001) 79–2727.

[13] P. Montmitonnet, Hot and cold strip rolling processes, Computer methods in applied mechanics and engineering 195 (2006) 6604–6625.

[14] M. Wang, H. Yang, Z. Sun, L. Guo, Analysis of coupled mechanical and thermal behaviors in hot rolling of large rings of titanium alloy using 3d dynamic explicit fem, Journal of Materials Processing Technology 209 (2009) 3384 – 3395.

[15] A. R. Shahani, S. Setayeshi, S. A. Nodamaie, M. A. Asadi, S. Rezaie, Prediction of influence parameters on the hot rolling process using finite element method and neural network, Journal of materials processing technology 209 (2009) 1920–1935.

[16] CEA, Cast3m, 2011. Commissariat A l'Energie Atomique, http://www-cast3m.cea.fr/.

[17] N. Muskhelishvili, Singular integral equations : boundary problems of function theory and their application to mathematical physics, Dover, New York, pp. 316–322. First edition (1953).

[18] M. Abbaspour, A. Saboonchi, Work roll thermal expansion control in hot strip mill, Applied Mathematical Modeling 32 (2008) 2652–2669.

Appendix A. Proof of the particular solution

The left term of (19) involves the following quantity:

$$g_1(r) = (\lambda + 2\mu)\left(P_n''(r) + \frac{P_n'(r)}{r} - \frac{P_n(r)}{r^2}\right) - \mu n^2 \frac{P_n(r)}{r^2} \tag{A.1}$$

By using (20) and denoting $x = \zeta_n r$:

$$g_1(r) = -(\lambda + 2\mu)L_n\left(J_n'''(x) + \frac{J_n''(x)}{x} - \frac{J_n'(x)}{x^2}\right) + \mu n^2 L_n \frac{J_n'(x)}{x^2}$$

The well known differential equation verified by Bessel function is:

$$J_n''(x) + \frac{J_n'(x)}{x} + \left(1 - \frac{n^2}{x^2}\right)J_n(x) = 0 \tag{A.2}$$

Therefore by differentiating (A.2):

$$J_n'''(x) + \frac{J_n''(x)}{x} - \frac{J_n'(x)}{x^2} = -\left(1 - \frac{n^2}{x^2}\right)J_n'(x) - \frac{2n^2}{x^3}J_n(x)$$

Hence:

$$g_1(r) = -L_n(\lambda + 2\mu)\left(\left(\frac{n^2}{x^2} - 1\right)J_n'(x) - \frac{2n^2}{x^3}J_n(x)\right) + L_n\mu n^2 \frac{J_n'(x)}{x^2}$$

And finally:

$$g_1(r) = -L_n\left((\lambda + \mu)\frac{n^2}{x^2} - (\lambda + 2\mu)\right)J_n'(x) + 2L_n(\lambda + 2\mu)\frac{n^2}{x^3}J_n(x) \tag{A.3}$$

The left term of (19) involves the following quantity:

$$g_2(r) = (\lambda + \mu)in\frac{Q_n'(r)}{r} - (\lambda + 3\mu)in\frac{Q_n(r)}{r^2}$$

By using (20):

$$g_2(r) = (\lambda + \mu)n^2 L_n\left(\frac{J_n'(x)}{x^2} - \frac{J_n(x)}{x^3}\right) - (\lambda + 3\mu)n^2 L_n \frac{J_n(x)}{x^3}$$

And finally:

$$g_2(r) = L_n(\lambda + \mu)\frac{n^2}{x^2}J_n'(x) - 2L_n(\lambda + 2\mu)\frac{n^2}{x^3}J_n(x) \tag{A.4}$$

By combining (A.3) and (A.4):

$$g_1(r) + g_2(r) = L_n(\lambda + 2\mu)J_n'(x) \tag{A.5}$$

Therefore the first Eq. of (19) is verified.

The left term of (19) involves the following quantity:

$$g_3(r) = \mu\left(Y_n''(r) + \frac{Q_n'(r)}{r} - \frac{Q_n(r)}{r^2}\right) - (\lambda + 2\mu)n^2\frac{Q_n(r)}{r^2}$$

By using (20):

$$g_3(r) = -inL_n\left(\mu\left(\frac{J_n''(x)}{x} - 2\frac{J_n'(x)}{x^2} + 2\frac{J_n(x)}{x^3} + \frac{J_n'(x)}{x^2} - \frac{J_n(x)}{x^3} - \frac{J_n(x)}{x^3}\right) - (\lambda + 2\mu)n^2\frac{J_n(x)}{x^3}\right)$$

Hence:

$$g_3(r) = -inL_n\left(\mu\left(\frac{J_n''(x)}{x} - \frac{J_n'(x)}{x^2}\right) - (\lambda + 2\mu)n^2\frac{J_n(x)}{x^3}\right)$$

By using directly (A.2):

$$g_3(r) = -inL_n\left(\mu\left(-2\frac{J_n'(x)}{x^2} + \left(\frac{n^2}{x^3} - \frac{1}{x}\right)J_n(x)\right) - (\lambda + 2\mu)n^2\frac{J_n(x)}{x^3}\right)$$

And:

$$g_3(r) = inL_n\left(2\mu\frac{J_n'(x)}{x^2} + \left((\lambda+\mu)\frac{n^2}{x^3} + \frac{\mu}{x}\right)J_n(x)\right) \tag{A.6}$$

The left term of (19) involves the following quantity:

$$g_4(r) = (\lambda+\mu)in\frac{P_n'(r)}{r} + (\lambda+3\mu)in\frac{P_n(r)}{r^2}$$

By using (20):

$$g_4(r) = -inL_n\left((\lambda+\mu)\frac{J_n''(x)}{x} + (\lambda+3\mu)\frac{J_n'(x)}{x^2}\right)$$

By using directly (A.2):

$$g_4(r) = -inL_n\left((\lambda+\mu)\left(-\frac{J_n'(x)}{x^2} + \left(\frac{n^2}{x^3} - \frac{1}{x}\right)J_n(x)\right) + (\lambda+3\mu)\frac{J_n'(x)}{x^2}\right)$$

And:

$$g_4(r) = inL_n\left(-2\mu\frac{J_n'(x)}{x^2} - (\lambda+\mu)\left(\frac{n^2}{x^3} - \frac{1}{x}\right)J_n(x)\right) \tag{A.7}$$

By combining (A.6) et (A.7):

$$g_3(r) + g_4(r) = inL_n(\lambda+2\mu)\frac{J_n(x)}{x} \tag{A.8}$$

Therefore the second Eq. of (19) is verified.

Appendix B. Temperature field

$$T_0 = 366.3 \tag{B.1}$$

Table B.4: T_n

n	T_n	n	T_n	n	T_n	n	T_n
1	-1.92D+01+i 2.05D+01	51	4.03D-03+i 3.48D-02	101	-1.84D-04+i 2.35D-03	151	-3.00D-07+i 3.41D-05
2	9.70D+00+i -1.44D+01	52	-1.22D-03+i 1.51D-02	102	1.59D-04+i 2.10D-03	152	-3.00D-07+i 3.16D-05
3	-2.76D+00+i 1.09D+01	53	-2.68D-03+i 3.25D-02	103	-1.49D-04+i 1.96D-03	153	-4.16D-09+i 2.69D-05
4	2.85D+00+i -5.46D+00	54	5.56D-03+i 1.47D-02	104	1.09D-04+i 1.96D-03	154	-5.00D-07+i 2.47D-05
5	-2.85D+00+i 4.36D+00	55	-7.51D-03+i 2.89D-02	105	-7.59D-05+i 1.66D-03	155	3.00D-07+i 2.12D-05
6	2.57D+00+i -2.51D+00	56	8.52D-03+i 1.63D-02	106	3.84D-05+i 1.79D-03	156	-3.00D-07+i 1.89D-05
7	-2.67D+00+i 2.63D+00	57	-9.28D-03+i 2.31D-02	107	-2.43D-05+i 1.42D-03	157	1.00D-07+i 1.66D-05
8	2.07D+00+i -1.59D+00	58	8.90D-03+i 1.83D-02	108	-1.56D-05+i 1.59D-03	158	-5.00D-07+i 1.42D-05
9	-1.40D+00+i 1.58D+00	59	-8.02D-03+i 1.72D-02	109	5.53D-05+i 1.27D-03	159	1.00D-07+i 1.28D-05
10	1.18D+00+i -4.43D-01	60	7.33D-03+i 2.01D-02	110	-6.74D-05+i 1.36D-03	160	-2.00D-07+i 1.06D-05
11	-8.89D-01+i 4.70D-01	61	-5.47D-03+i 1.35D-02	111	9.36D-05+i 1.14D-03	161	-5.84D-08+i 9.70D-06
12	7.84D-01+i 2.31D-01	62	4.12D-03+i 2.03D-02	112	-9.22D-05+i 1.16D-03	162	2.61D-08+i 8.00D-06
13	-6.40D-01+i 4.21D-03	63	-2.54D-03+i 1.12D-02	113	7.73D-05+i 1.03D-03	163	-1.00D-07+i 7.20D-06
14	4.80D-01+i 3.21D-01	64	9.74D-04+i 1.86D-02	114	-6.81D-05+i 9.83D-04	164	1.97D-08+i 5.90D-06
15	-1.91D-01+i -8.82D-02	65	2.79D-04+i 1.06D-02	115	3.82D-05+i 9.28D-04	165	-9.91D-08+i 5.10D-06
16	5.59D-02+i 3.80D-01	66	-1.19D-03+i 1.61D-02	116	-3.58D-05+i 8.21D-04	166	1.00D-07+i 4.30D-06
17	1.03D-01+i -1.90D-01	67	2.00D-03+i 1.14D-02	117	2.71D-05+i 8.36D-04	167	-7.95D-08+i 3.70D-06
18	-1.71D-01+i 4.18D-01	68	-2.48D-03+i 1.32D-02	118	-1.35D-05+i 7.05D-04	168	5.29D-08+i 3.10D-06
19	1.87D-01+i -1.73D-01	69	2.47D-03+i 1.21D-02	119	4.00D-06+i 7.15D-04	169	-7.04D-08+i 2.60D-06
20	-2.16D-01+i 2.96D-01	70	-2.38D-03+i 1.04D-02	120	9.70D-06+i 6.13D-04	170	3.67D-09+i 2.20D-06

21	2.49D-01+i -3.44D-02	71	2.03D-03+i 1.24D-02	121	-2.47D-05+i 6.08D-04	171	-1.90D-08+i 1.80D-06
22	-2.63D-01+i 1.53D-01	72	-1.40D-03+i 8.20D-03	122	2.45D-05+i 5.38D-04	172	5.27D-09+i 1.50D-06
23	2.72D-01+i 5.34D-02	73	1.03D-03+i 1.23D-02	123	-2.86D-05+i 5.13D-04	173	8.01D-09+i 1.20D-06
24	-2.55D-01+i 8.43D-02	74	-4.27D-04+i 6.90D-03	124	1.95D-05+i 4.71D-04	174	-4.97D-09+i 1.00D-06
25	2.08D-01+i 9.11D-02	75	-3.67D-05+i 1.13D-02	125	-2.20D-05+i 4.25D-04	175	4.88D-09+i 8.00D-07
26	-1.66D-01+i 3.07D-02	76	4.67D-04+i 6.42D-03	126	1.49D-05+i 4.17D-04	176	-1.64D-08+i 7.00D-07
27	1.22D-01+i 1.33D-01	77	-8.59D-04+i 9.91D-03	127	-1.06D-05+i 3.48D-04	177	4.29D-09+i 5.00D-07
28	-8.95D-02+i -1.52D-02	78	1.19D-03+i 6.44D-03	128	7.60D-06+i 3.57D-04	178	-1.50D-08+i 4.00D-07
29	6.20D-02+i 1.42D-01	79	-1.29D-03+i 8.38D-03	129	-4.30D-06+i 2.97D-04	179	-2.92D-09+i 3.00D-07
30	-4.19D-02+i -9.93D-03	80	1.21D-03+i 6.46D-03	130	1.90D-06+i 3.03D-04	180	-2.20D-09+i 2.00D-07
31	1.19D-02+i 1.10D-01	81	-1.14D-03+i 6.91D-03	131	6.80D-06+i 2.50D-04	181	1.09D-09+i 2.00D-07
32	6.29D-03+i 2.21D-02	82	8.84D-04+i 6.51D-03	132	-5.50D-06+i 2.52D-04	182	-4.57D-09+i 1.00D-07
33	-2.92D-02+i 7.31D-02	83	-6.24D-04+i 5.66D-03	133	6.90D-06+i 2.15D-04	183	-1.11D-09+i 1.00D-07
34	3.53D-02+i 4.31D-02	84	4.10D-04+i 6.28D-03	134	-8.20D-06+i 2.03D-04	184	2.60D-10+i 7.61D-08
35	-3.99D-02+i 4.47D-02	85	-2.08D-04+i 4.84D-03	135	5.40D-06+i 1.81D-04	185	-1.40D-10+i 5.61D-08
36	3.32D-02+i 6.25D-02	86	-3.77D-05+i 5.82D-03	136	-4.90D-06+i 1.66D-04	186	6.48D-11+i 3.84D-08
37	-2.99D-02+i 1.83D-02	87	2.35D-04+i 4.39D-03	137	2.30D-06+i 1.54D-04	187	-6.59D-10+i 2.74D-08
38	2.01D-02+i 8.18D-02	88	-4.16D-04+i 5.09D-03	138	-1.50D-06+i 1.35D-04	188	-4.24D-11+i 1.81D-08
39	-1.82D-02+i -1.74D-05	89	5.60D-04+i 4.18D-03	139	-4.00D-07+i 1.32D-04	189	-8.39D-11+i 1.19D-08
40	8.82D-03+i 8.38D-02	90	-6.12D-04+i 4.36D-03	140	-6.00D-07+i 1.11D-04	190	-3.47D-11+i 7.63D-09
41	-4.06D-03+i -1.77D-03	91	5.89D-04+i 3.99D-03	141	-1.50D-06+i 1.07D-04	191	-2.98D-11+i 4.50D-09
42	-4.54D-03+i 7.31D-02	92	-5.28D-04+i 3.68D-03	142	1.20D-06+i 9.23D-05	192	-1.24D-11+i 2.64D-09
43	1.06D-02+i 6.48D-03	93	4.30D-04+i 3.81D-03	143	-2.30D-06+i 8.69D-05	193	-7.06D-12+i 1.39D-09
44	-1.61D-02+i 5.99D-02	94	-3.37D-04+i 3.09D-03	144	3.00D-06+i 7.52D-05	194	-5.10D-12+i 7.04D-10
45	1.71D-02+i 1.43D-02	95	2.48D-04+i 3.56D-03	145	-2.40D-06+i 6.91D-05	195	1.80D-12+i 3.12D-10
46	-1.77D-02+i 4.46D-02	96	-1.53D-04+i 2.66D-03	146	2.60D-06+i 6.15D-05	196	-1.70D-12+i 1.24D-10
47	1.60D-02+i 2.34D-02	97	6.77D-05+i 3.17D-03	147	-1.70D-06+i 5.40D-05	197	8.93D-14+i 3.91D-11
48	-1.33D-02+i 2.98D-02	98	1.11D-05+i 2.43D-03	148	9.00D-07+i 5.02D-05	198	-3.59D-14+i 9.09D-12
49	1.09D-02+i 3.22D-02	99	-1.07D-04+i 2.75D-03	149	-1.30D-06+i 4.32D-05	199	2.09D-14+i 1.15D-12
50	-8.12D-03+i 1.99D-02	100	1.28D-04+i 2.24D-03	150	-9.70D-08+i 4.04D-05	200	-9.70D-16+i 3.49D-14

Table B.5: γ_n

n	$\gamma_n/(T_a - T_0)$	n	$\gamma_n/(T_a - T_0)$	n	$\gamma_n/(T_a - T_0)$
1	1.6017603	11	0.4198340	21	0.2792925
2	-1.0640481	12	-0.3994332	22	-0.2697257
3	0.8499229	13	0.3812070	23	0.2605739
4	-0.7272953	14	-0.3647408	24	-0.2517861
5	0.6451733	15	0.3497198	25	0.2433180
6	-0.5850795	16	-0.3359009	26	-0.2351319
7	0.5385006	17	0.3230924	27	0.2271942
8	-0.5009022	18	-0.3111410	28	-0.2194761
9	0.4696192	19	0.2999224	29	0.2119517
10	-0.4429698	20	-0.2893344	30	-0.2045984
n	$\gamma_n/(T_a - T_0)$	n	$\gamma_n/(T_a - T_0)$	n	$\gamma_n/(T_a - T_0)$
31	0.1973955	41	0.1303318	51	0.0651469
32	-0.1903252	42	-0.1238687	52	-0.0584356
33	0.1833701	43	0.1174123	53	0.0516561
34	-0.1765158	44	-0.1109563	54	-0.0448147
35	0.1697488	45	0.1044914	55	0.0378854
36	-0.1630565	46	-0.0980124	56	-0.0308898
37	0.1564265	47	0.0915102	57	0.0237728

38	-0.1498492	48	-0.0849808	58	-0.0166182
39	0.1433137	49	0.0784137	59	0.0091932
40	-0.1368109	50	-0.0718065	60	-0.0026463